Steel and Composite Structures, *Vol. 28, No. 5 (2018) 527-539*
DOI: https://doi.org/10.12989/scs.2018.28.5.527

Seismic behavior of SFRC shear wall with CFST columns

Dan-Ying Gao [1,2a], Pei-Bo You [*1,3], Li-Juan Zhang [1b] and Huan-Huan Yan [1c]

[1] *Research Center of New Style Building Material & Structure, Zhengzhou University, Zhengzhou 450001, China*
[2] *College of Civil Engineering, Henan University of Engineering, Zhengzhou 451191, China*
[3] *Henan University of Urban Construction, Pingdingshan 467000, China*

(*Received November 2, 2017, Revised June 28, 2018, Accepted July 4, 2018*)

Abstract. The use of reinforced concrete (RC) shear wall with concrete filled steel tube (CFST) columns and steel fiber reinforced concrete (SFRC) shear wall has aroused widespread attention in recent years. A new shear wall, named SFRC shear wall with CFST columns, is proposed in this paper, which makes use of CFST column and SFRC shear wall. Six SFRC shear wall with CFST columns specimens were tested under cyclic loading. The effects of test parameters including steel fiber volume fraction and concrete strength on the failure mode, strength, ductility, rigidity and dissipated energy of shear wall specimens were investigated. The results showed that all tested shear wall specimens exhibited a distinct shear failure mode. Steel fibers could effectively control the crack width and improve the distribution of cracks. The load carrying and energy dissipation capacities of specimens increased with the increase of steel fiber volume fraction and concrete strength, whilst the ductility of specimens increased with the increase of steel fiber volume fraction and the decrease of concrete strength.

Keywords: concrete filled steel tube columns; shear wall; steel fiber reinforced concrete; seismic behavior; ductility; dissipated energy

1. Introduction

Reinforced concrete (RC) shear wall structure can gain better seismic performance through the reasonable design, and is commonly used in high rise buildings in the past decade. Many high-rise buildings over 100 m tall have been constructed in China with the increase of demands. Both the axial force and bending moment, which are assigned to the RC shear wall on ground floor, increase with the height increase of high-rise building. The thick RC shear walls and boundary elements with high reinforcement ratio are usually used in order to meet the demands of axial compression ratio, load bearing capacity and deformation, which increases the construction difficulty and reduces the usable area of building. In particular, the transverse dimension of shear wall can be decreased with the application of high strength concrete, but the brittleness of reinforced high strength concrete (RHSC) shear wall increases inevitably. Correspondingly, the higher requirement for the seismic behavior of RHSC shear wall would be put forward. Nowadays, the research work focuses on the following two aspects to get better seismic behavior of RHSC shear wall.

Firstly, the ductility of RHSC shear walls is improved through the structural innovation. Among the methods used, the RHSC shear wall with concrete filled steel tube (CFST) columns is an efficient method, which has gained the increasing popularity in engineering practice (Xiao *et al*. 2012, Li *et al*. 2015). Theoretical analysis and experimental study (Liao *et al*. 2009, Cao *et al*. 2011, Huang *et al*. 2012, Qu *et al*. 2015, Hu *et al*. 2016) show that the CFST columns serving as boundary members can provide the effective constraint to RHSC wall, restrain the cracking development, and also bear part of transverse load after the RHSC wall deteriorates gradually, indicating that the RHSC shear wall with CFST columns can form double-channel seismic line and have favorable seismic performance.

Secondly, the application of steel fiber reinforced concrete (SFRC) is a good way to enhance the seismic behavior of conventional shear wall structure, especially the RHSC shear wall. Several researchers (Tang *et al*. 1993, Zhao *et al*. 2009, Zhao and Dun 2014, Eom *et al*. 2014) have conducted the experiments on the seismic performance of SFRC shear wall. In these experiments, the SFRC shear walls were subjected to reversed cyclic loading. As expected, because SFRC has good properties, such as stretching, shear resistance, cracking resistance, toughness, fire resistance, earthquake resistance and so on (Gao *et al*. 2017a, b, Mirsayah and Banthia 2002, Zerbino and Barragan 2012, Singh and Kaushik 2001, Kang *et al*. 2012, Saridemir *et al*. 2017, Tang 2017, Xia and Naaman 2002, Eltobgy 2013, Cai *et al*. 2016), it can remarkably improve the seismic behavior of RC shear wall, and reduce the phenomenon of reinforcement congestion and construction difficulty. The load bearing capacity, ductility and energy dissipation capacities of SFRC shear walls increase with the increasing of steel fiber volume fraction.

In this paper, a new kind of double composite shear wall

*Corresponding author, Ph.D.,
E-mail: 382618232@qq.com
[a] Professor, E-mail: gdy@zzu.edu.cn
[b] Lecturer, E-mail: floycn526@163.com
[c] Ph.D., E-mail: 930257335@qq.com

http://www.techno-press.org/?journal=scs&subpage=6
ISSN: 1229-9367 (Print), 1598-6233 (Online)

is introduced, which includes SFRC web and CFST boundary elements. In this new composite shear wall, SFRC web can improve its ductility and energy dissipation capacities, CFST boundary elements can enhance its load bearing capacity. This kind of composite shear wall can adequately make use of the advantages of SFRC shear web and CFST columns. In order to fully understand the seismic behavior of the new structure, six SFRC shear wall with CFST columns specimens were designed and tested. The test parameters consisted of concrete strength grade (CF40, CF60, CF80) and steel fiber volume fraction (0, 0.5%, 1.0%, 1.5%). The experimental programme, results and analysis are presented in the followings.

2. Test programme

2.1 Specimen design

Six shear wall specimens were fabricated with the same dimensions and configurations. Each mainly consists of five parts, one SFRC web in the center, two CFST columns that lie in the right and left sides of web, several U-shaped connectors welded to CFST columns, one RC top beam and one RC foundation beam, as shown in Figs. 1(a)-(c).

The height and thickness of shear walls were 600 and 120 mm, respectively. For comparison purposes, the size and reinforcement ratio of SFRC webs were kept the same. For all shear walls, both the horizontal and vertical reinforcing bars of 6 mm diameter consisted of two layers, the reinforcement ratio of horizontal and vertical reinforcing bars was approximately 0.55%. The sectional dimension of square CFST columns was $a \times a \times t = 120 \times 120 \times 3$ mm, where a and t were the length and thickness of steel tubes, respectively.

All specimens were designed as shear-dominant failure mode. The distance from the loading point to the top surface of the foundation beam was 750 mm, the ratio of shear span to depth herein was 1.0 for all specimens. Due to the limitations of test equipment, the size of tested specimens was approximately designed as one-fourth scale of the prototype structure.

The top beam for all shear wall specimens had a section of 250 mm width by 300 mm height, and the foundation beam had a section of 450 mm width by 500 mm height, which was mounted on the base of specimens. The detailed steel bar configurations of top beam and foundation beam are all shown in Fig. 1(a).

The target axial compression ratio, n', was designed as 0.2, while the corresponding target axial compressive force, N, for each shear wall specimen was calculated by Eq. (1) (Cao *et al*. 2011).

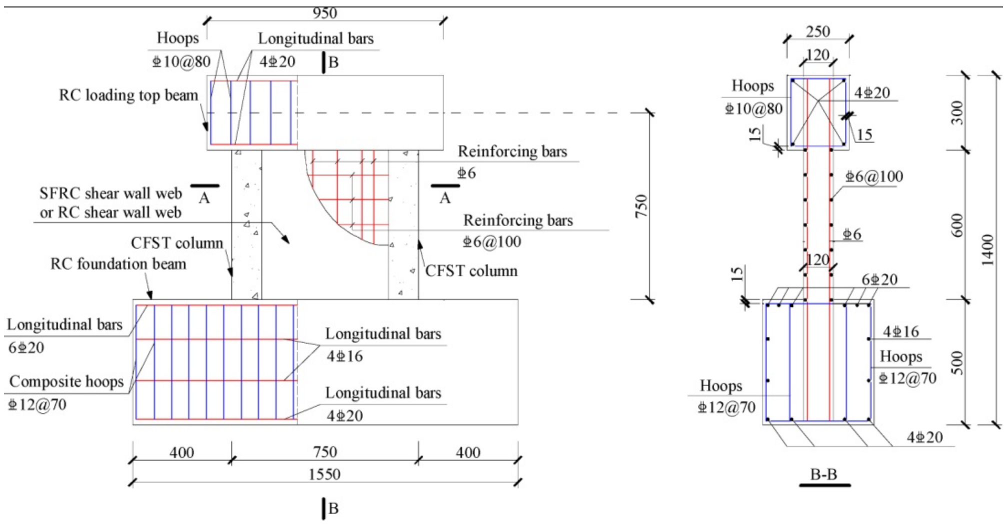

(a) Elevation

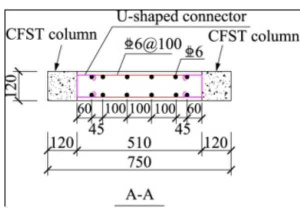

(b) A-A section

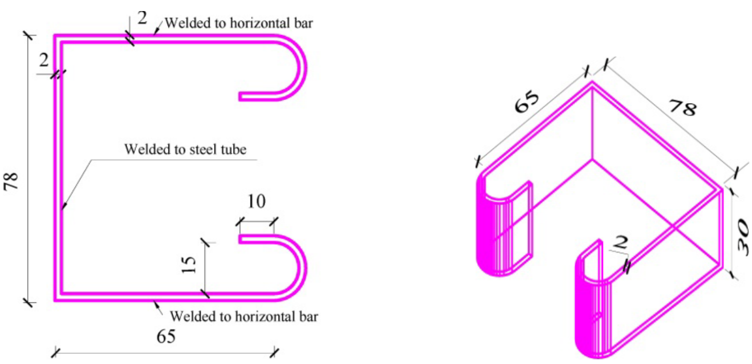

(c) One-dimensional and three-dimensional graph of U-shaped connector

Fig. 1 Specimen configuration (Unit: mm)

$$N = n'\left[f_c' \left(A_c - 8at \right) + 8 f_c' E_s' at \big/ E_c' \right] \tag{1}$$

where f_c' is the target axial compressive strength of concrete, A_c is the cross sectional area of shear wall web, A_c = 120 mm × 750 mm, E_s' and E_c' is the elastic modulus of target steel tube and target concrete, respectively. The corresponding target axial compressive force calculated by Eq. (1) is listed in Table 1 for each specimen. Since the mean axial compressive strength of concrete, f_c, is generally larger than the target axial compressive strength of concrete, the mean axial compression ratio, n, is lower than the target axial compression ratio.

Table 1 Parameters of shear wall specimens

Specimen designation	Target axial compressive force N (kN)	Steel fiber volume fraction ρ_f(%)	Target concrete compressive strength f_c' (MPa)
SS-1.0-00-C60	567	0	60
SS-1.0-05-CF60	567	0.5	60
SS-1.0-10- CF60	567	1.0	60
SS-1.0-15- CF60	567	1.5	60
SS-1.0-10- CF40	394	1.0	40
SS-1.0-10- CF80	740	1.0	80

Table 2 Material properties of steel plate and bar

Type	Yield strength f_y (MPa)	Ultimate strength f_u (MPa)	Elastic modulus E_s (MPa)
3 mm plate	307.67	392.00	1.98×10^5
2 mm plate	236.67	323.20	1.88×10^5
C 6 bar	369.17	521.60	1.85×10^5

Table 3 Properties of steel fiber

Type	Nominal diameter d_f (mm)	Length l_f(mm)	Aspect ratio l_f / d_f	Tensile strength f_{sf} (MPa)
3D 65/35BG	0.55 ± 10%	35 ± 10%	64	1345 ± 15%

More details of each shear wall specimen are given in Table 1. For the specimen designations in Table 1, SS represents the steel tube and steel fiber used, a number 1.0 refers to the ratio of shear span to depth, and the next number represents the steel fiber volume fraction of the web in shear wall. Target concrete compressive strength starting with C represents plain concrete, whilst CF represents SFRC, and the last number denotes the target concrete compressive strength of shear wall specimen.

2.2 Material properties and mixture proportion of concrete

The steel plates for the hollow sections of square CFST columns are made by the cold-formed steel tubes with the thickness of 3 mm. The steel plates cut from sheets were bent into the U-shaped connectors as shown in Fig. 1(c). The strength grade of reinforcing bars was HRB400, the grade of steel plates for tubes and sheets was Q235B. The yield strength, ultimate strength and elastic modulus of steel plates and reinforcing bar were measured by the tensile tests according to Chinese Standard (GB/T 228.1-2010). The measured properties of steel plate and bar are given in Table 2.

Ordinary Portland cement P.O. 42.5 according to Chinese Standard was used in all specimens, which was produced by Tianrui Group Zhengzhou Cement Co., Ltd. The crushed limestone with the continuous particle size distribution from 5 mm to 20 mm was used as coarse aggregate. The natural river sand with a fineness modulus of 2.70 and maximum particle size of 5 mm was used as fine aggregate. The domestic water was utilized in the production of concrete. Poly carboxylic acid water reducing agent (WRA) produced by Sobute New Materials Co., Ltd. was used to maintain the workability of fresh concrete, the water-reducing rate was 20%~30%. The dramix steel fiber (SF) produced by Bekaert Applied Material Technology (Shanghai) Co., Ltd. was used in SFRC as reinforcing material, which belongs to low carbon hooked steel fiber. The properties of steel fiber provided by the manufacturer are detailed in Table 3.

The SFRC mixture proportions in the web for all shear wall specimens are given in Table 4. The concrete of the CFST columns, top beam and foundation beam for each shear wall specimen was plain concrete which had the

Table 4 Mixture proportion design of concrete

Target concrete compressive strength	Cement (kg/m^3)	Water (kg/m^3)	SF (kg/m^3)	Sand (kg/m^3)	Aggregate (kg/m^3)	WRA (kg/m^3)	SF volume fraction
C(F)40	441	211	0	718	1078	0.882	0%
	441	211	78	718	1078	0.882	1.0%
C(F)60	529	164	0	646	1110	5.819	0%
	529	164	39	646	1110	5.819	0.5%
	529	164	78	646	1110	5.819	1.0%
	529	164	117	646	1110	5.819	1.5%
C(F)80	582	159	0	595	1108	7.391	0%
	582	159	78	595	1108	7.391	1.0%

similar mixture proportion as the SFRC in the shear wall web.

2.3 Specimen fabrication

The fabricating process of the steel frames of shear wall specimens was mainly divided into four steps, as shown in Fig. 1: Firstly, the steel tubes and the U-shaped connectors were made according to designed size, then a series of close ends of the U-shaped connectors with equal spacing as horizontal reinforcements were welded to the tube wall of steel tubes to insure the effective connections between steel tubes and web (Shirali 2002, Vetr *et al*. 2016, Qiao *et al*. 2017, Xu *et al*. 2017). Secondly, the reinforcing cage of foundation beam was fabricated. Two prefabricated steel tubes with U-shaped connectors were fixed in the reinforcing cage of the foundation beam according to determined distance. Thirdly, the horizontal and vertical reinforcements of web were assembled. The horizontal reinforcements were welded to the two distal ends of U-shaped connector. Finally, the reinforcing cage of top beam was fabricated. The completed steel frame and U-shaped connector are presented in Figs. 2(a)-(b), respectively.

(a) Steel frame (b) U-shaped connector

Fig. 2 Steel frame and U-shaped connector

Prior to concrete casting, the plywood was used to manufacture the formwork. The concrete in the CFST columns was the plain concrete and was cast firstly. One week later, the concrete in the web, top beam and foundation beam of shear wall was cast. At the same time, the six prism specimens with size of 150 mm × 150 mm × 300 mm and six cubic specimens with size of 150 mm were cast for compressive and splitting tensile tests. The mechanical properties of concrete for the columns and web of shear wall specimens are listed in Table 5.

2.4 Experimental methodology

2.4.1 Test set-up

The detailed test set-up is illustrated in Figs. 3(a)-(b). The specimen was placed in the vertical steel frame of testing machine. The foundation beam of shear wall specimen was fixed on the rigid floor by ground anchor. A 2000 kN vertical hydraulic jack was used to provide the axial compressive force for each specimen. The top end of hydraulic jack was connected to the vertical steel frame by one rolling support, which permitted the shear wall to move freely in lateral direction and made the axial compressive force be applied to the center of specimens all the time. The

Table 5 Prismatic compressive strength and tensile strength of concrete and SFRC

Specimen designation	For concrete in column		For concrete and SFRC in web	
	f_c (MPa)	f_t (MPa)	f_c (MPa)	f_t (MPa)
SS-1.0-00-C60	55.9	2.76	56.3	2.81
SS-1.0-05-CF60	55.5	2.73	55.2	3.67
SS-1.0-10-CF60	55.5	2.74	55.1	6.15
SS-1.0-15-CF60	56.0	2.77	56.5	7.88
SS-1.0-10-CF40	38.1	2.15	38.3	3.78
SS-1.0-10-CF80	64.6	3.96	65.6	6.84

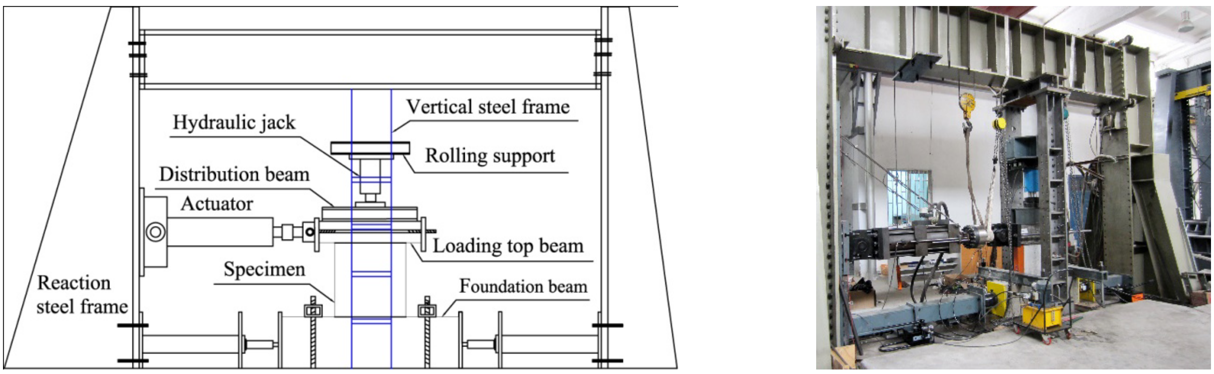

(a) Schematic view (b) Test scene

Fig. 3 Test set-up

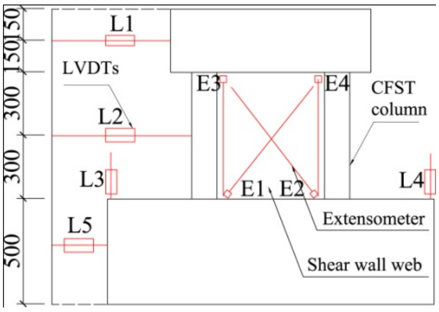

(a) LVDTs and extensometers

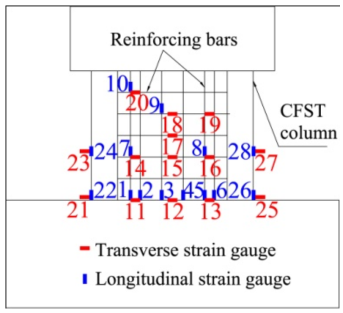

(b) Strain gauges

Fig. 4 Instrumentation of specimens

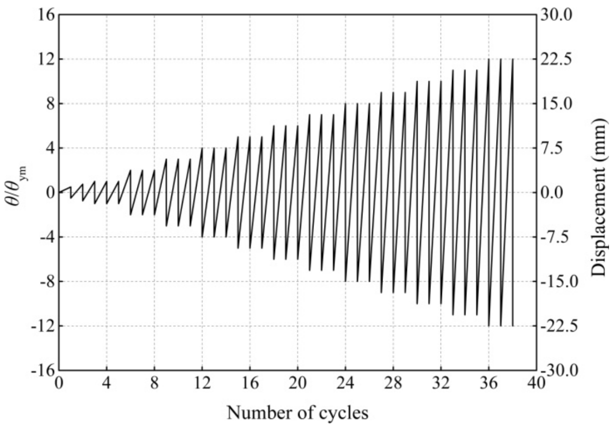

Fig. 5 Loading history

lower end of vertical jack was placed on the distribution beam, which was located on the top of top beam. The lateral load was cyclically applied along the centerline of top beam of specimen through an electro-hydraulic servo control actuator with a maximum force of ±1500 kN and a maximum stroke of ±125 mm.

The measuring instrument layout for each shear wall specimen was the same, as shown in Figs. 4(a)-(b). Three horizontal linear variable differential transformers (LVDTs) were used to get the lateral displacements at the different heights of specimen. The top horizontal LVDTs L1 measured the lateral displacement along the centerline of top beam, the middle one L2 measured the lateral displacement along the middle height of shear wall, and the lower one L5 was used to get the slip of foundation beam in lateral force direction. Meanwhile, two vertical LVDTs L3 and L4 mounted on foundation beam were used to measure the rotation of foundation beam. Two diagonal extensometers E1 and E2 and two vertical extensometers E3 and E4 fixed on the web were used to measure the shear and flexural deformations, respectively. A series of strain gauges were used to gain the strains in reinforcing bars and steel tubes, the positions of strain gauges are shown in Fig. 4(b). The strain gauges numbered 1-10 and 11-20 were used to get the strains in vertical and horizontal reinforcing bars, respectively. The strain gauges numbered 21-28 were used to get the strains in steel tubes.

The lateral and vertical loads were automatically collected through the loading cells in hydraulic actuator and jack, respectively. The cracking of web and the buckling of CFST columns were also observed and recorded with handwork during the test. The maximum crack width of web was measured by DJCK-2 crack instrument. The data of load, displacement and strain were collected by DH3816 static data acquisition system produced by Donghua Testing Technology Co., Ltd.

2.4.3 Loading history

Each specimen was tested under constant axial force and cyclic lateral load. The axial compressive force N given in Table 1 was applied first and maintained constant during test process. Subsequently, the tests were conducted under the rotation controlled cyclic loading until the lateral load reduced below 85% of peak lateral load (P_m). Rotation control is usually a loading method by the multiple of yield rotation angle. A typical rotation controlled cyclic loading history is presented in Fig. 5. Since it is difficult to accurately determine the yield rotation angle of the shear wall specimens before the experiment, a nominal yield rotation angle was mainly designated before the experiment in some previous experimental studies (Liao *et al*. 2009, Hu *et al*. 2016). A maximum elastic inter-story rotation angle of steel-concrete mixed structure of tall buildings was taken as a nominal yield rotation angle herein. Therefore, a nominal yield rotation angle (θ_{ym}) was taken as 1/400 rad according to Chinese Standard CECS 230:2008 (CECS 230:2008), which was corresponding to a nominal yield lateral displacement (Δ_{ym}) at the loading point, $\Delta_{ym} = \theta_{ym} \times 750$ mm = 1.875 mm. Prior to θ_{ym}, two rotation levels of $0.5\theta_{ym}$ and $0.75\theta_{ym}$ were imposed. Hereafter, the rotation increment was 1/400 rad for each rotation level and three cycles were imposed at each rotation level. In addition, the nominal yield load was the mean value of positive and negative loads when the corresponding lateral displacements of specimens were ±1.875 mm.

3. Test results and discussion

3.1 Damage and failure mode

The failure pattern and crack distribution at peak and ultimate state (the lateral force degraded to 85% of the P_m) of all tested shear wall specimens are shown in Figs. 6(a)-(c). It could be found that all specimens mainly showed a typical diagonal cracking pattern during test process and

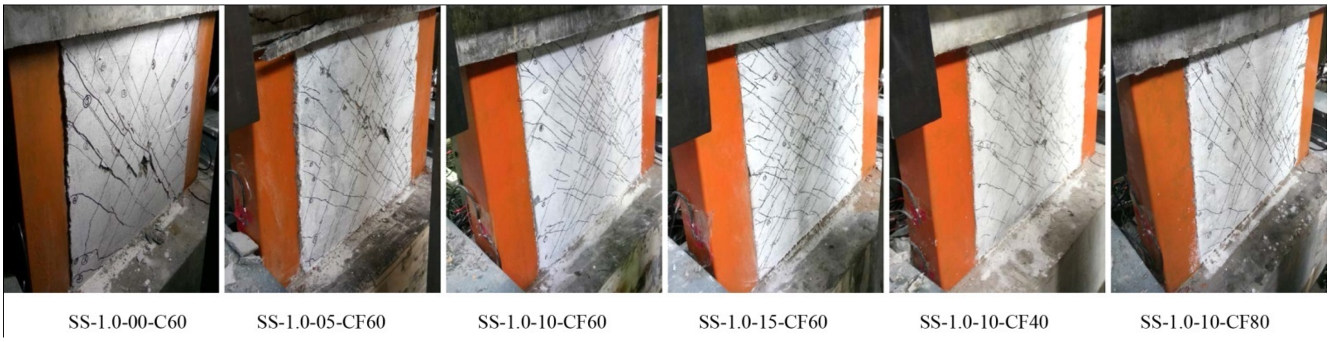

(a) Failure pattern at peak state

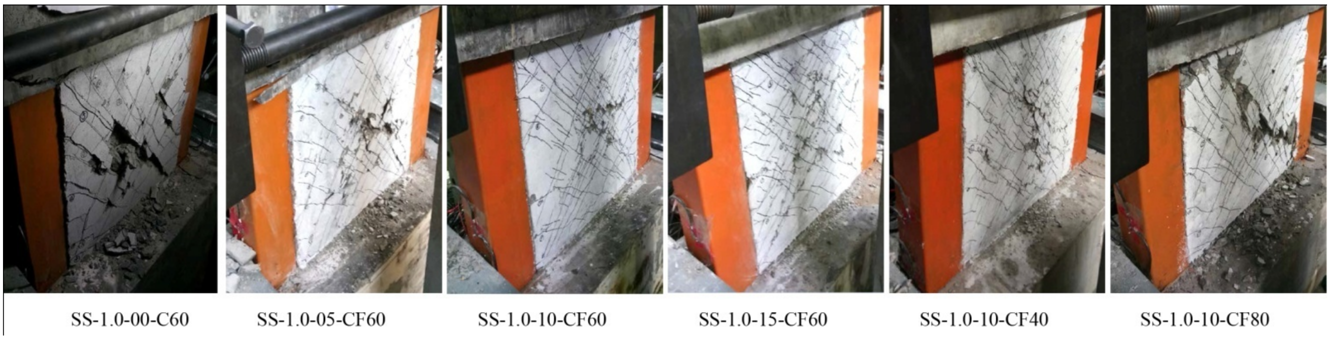

(b) Failure pattern at ultimate state

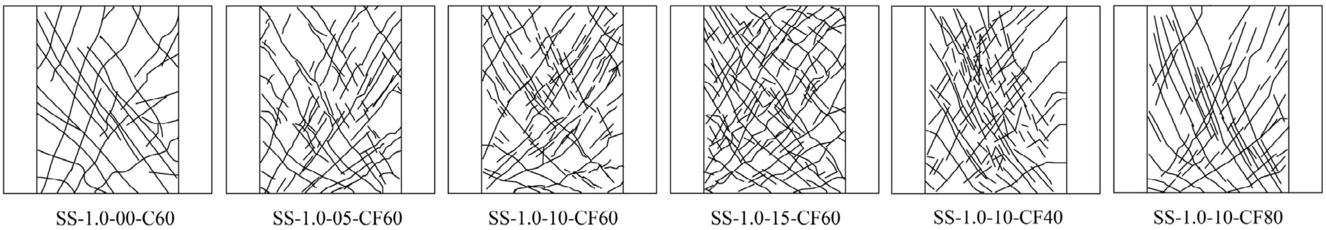

(c) Schematic view of crack distribution

Fig. 6 Failure pattern and crack distribution of shear wall specimens

their failure mode was shear-dominant.

The specimen SS-1.0-00-C60 was selected as an example to demonstrate the experimental observations during the whole loading process. The first observed crack occurred at the right corner of the web bottom during the controlled rotation of $3\theta_{\mathrm{ym}}$. This first crack caused by shear stress was 0.12 mm in width, then extended along an angle around 45° to the horizontal direction to the mid portion of web. As the test went on, many new inclined cracks gradually appeared, and the existing cracks constantly extended under the action of cyclic loading. For the $9\theta_{ym}$ cycle, several pairs of visible intercrossing diagonal cracks with a maximum width of 0.52 mm developed approximately along the diagonal directions of web. The web was divided into a series of concrete blocks by the diagonal cracks. In this stage, no obvious local buckling occurred on the steel tubes, but the measured strains of reinforcements were more than 0.002, which indicated that the reinforcements at the middle part of the web and steel tubes at the bottom of columns had yielded. For the $11\theta_{ym}$ cycle, the RC shear wall specimen reached its P_m, many new inclined cracks at the top corners and middle part of web appeared, and the crack patterns at this moment are shown in Fig. 6(a). Furthermore, the maximum width of the cracks at the middle part of web increased rapidly and even reached to 2.0 mm. Meanwhile, the minor spalling of concrete happened at the middle part of web and the slight local buckling of the square steel tube on the right side was observed. The measured strains of horizontal reinforcements in the web indicated that almost all of them yielded by tension. Hereafter, new cracks seldom occurred, but the widths of inclined cracks and the strains of reinforcements at the middle part of web developed rapidly upon further loading. After the P_m, the carrying capacity of the RC shear wall specimen decreased significantly. For the $13\theta_{ym}$ cycle, the surface concrete at the middle part of web was crushed and spalled, and the reinforcing bars were exposed, the shear force transferred quickly from web to CFST columns, so the degree of local buckling of steel tubes at the bottom of RC shear wall increased continuously and formed a more concentrated energy dissipation region, as shown in Fig. 7. As a result, the lateral load reduced rapidly to about 85% of P_m, indicating the failure of specimen and the ending of test. The whole damage process of RC shear wall specimen exhibited a distinct brittle failure. The final failure patterns of specimens are given in Fig. 6(b).

Fig. 7 Local buckling of steel tube at the bottom of specimen SS-1.0-00-C60

When steel fibers were added to the web in RC shear wall, the final failure appearance of SFRC shear wall specimen was similar to that of RC shear wall specimen, as shown in Fig. 6. From the test observations, all the shear wall specimens showed a shear-dominant failure mode and mainly exhibited a typical diagonal cracking pattern. Despite steel fiber volume fraction was different, the failure process of the specimens was similar and could be divided into four stages: initial cracking stage, main diagonal cracks forming stage, peak load stage and failure stage. However, steel fibers significantly affected the crack development and distribution in the wall web, the failure speed of shear wall specimens and the degree of local buckling on the square steel tubes. It confirmed from the tests that the reinforcing effect of steel fiber on the behavior of RC shear wall specimen was related to its volume fraction. The SFRC web in shear wall behaved predominantly small cracks and micro cracks with smaller width, more quantity, higher density and wider distribution as the volume fraction of steel fiber increased. Meanwhile, the larger the steel fiber volume fraction, the higher loading cycle number of the SFRC shear wall specimen was, the later the P_m and the ultimate load (P_u) reached, and the better the ductility was. In brief, the crack in SFRC web was thin and densely covered, and developed slowly. For instance, the maximum crack width of RC shear wall specimen numbered SS-1.0-00-C60 was 2.0 mm, whilst the maximum crack width of SFRC shear wall specimen numbered SS-1.0-05-CF60, SS-1.0-10-CF60 and SS-1.0-15-CF60 was 1.6 mm, 1.2 mm and 1.0 mm, respectively. This is because the steel fiber in concrete can restrict the growth and widening of diagonal cracks in web, increase the area of shear-compression zone and aggregate interlock forces, the similar results were reported in literature (Zhao *et al*. 2009). Furthermore, the steel fiber can bear a part of shear force, increase the dowel action of reinforcement and improve the bond properties between steel bar and concrete, which was similar with the results in literature (Tang *et al*. 1993, Zhao *et al*. 2009, Eom *et al*. 2014).

As shown in Fig. 6, SFRC shear wall specimens with different concrete strength grade had similar failure appearance at peak and ultimate state under the condition of same steel fiber volume fraction. It could be found that the lateral load of SFRC shear wall specimen with higher concrete strength grade deteriorated more obviously after P_m, the crushing and spalling of concrete was more serious at ultimate state, especially for the specimen SS-1.0-10-CF80.

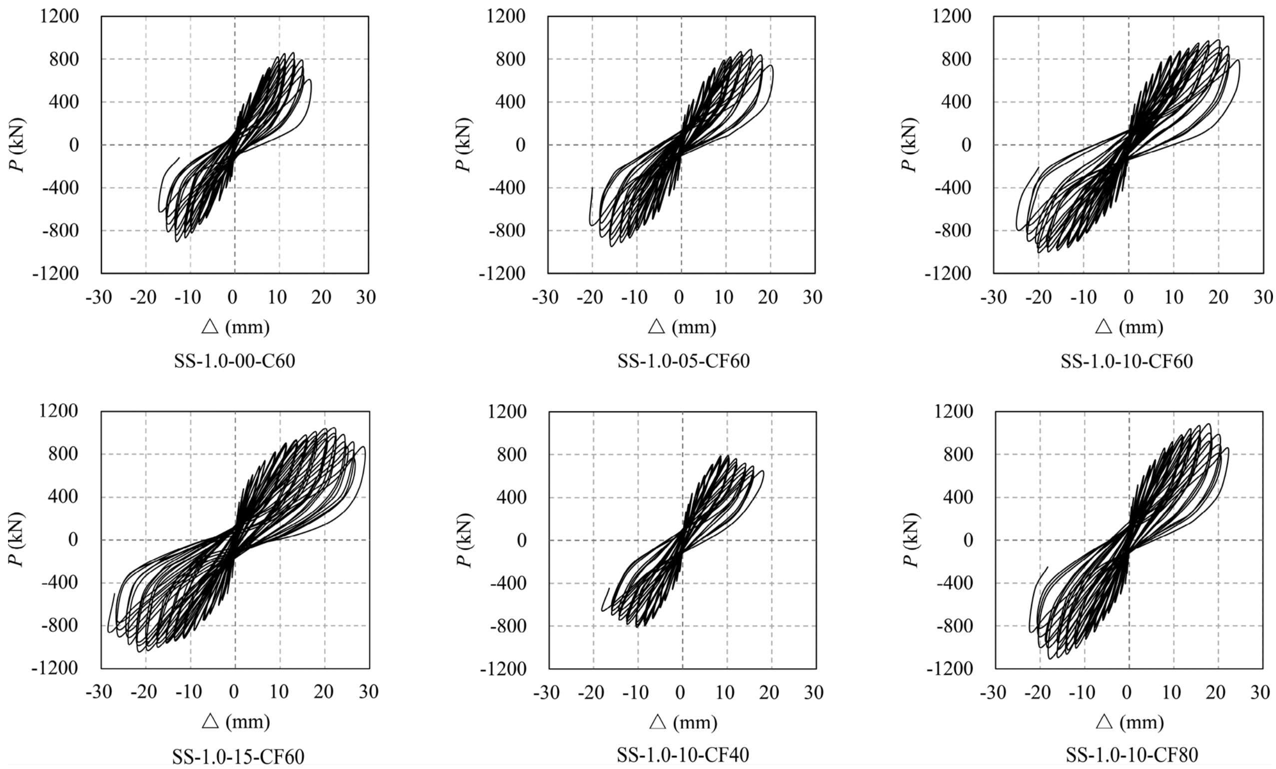

Fig. 8 P versus Δ hysteretic curves

During the test process, the connections between the square steel tubes and web were effective, no significant slip at the interface occurred, which indicated that the performance of the U-shaped connector designed was effective. Moreover, no obvious local buckling on the square steel tubes of SFRC shear wall specimens was observed at ultimate state. The SFRC shear wall specimens had the small degree of destruction compared with that without steel fibers, which indicated that the SFRC shear wall specimens had better repairability.

3.2 Lateral load (P) versus lateral displacement (Δ) hysteretic curves

The collected P versus Δ#hysteresis curves for each specimen are given in Fig. 8. It could be found that the hysteretic curves of SFRC shear wall specimens had a significant pinch phenomenon. Before the concrete cracking, the load-displacement curves changed almost straightly and no residual displacement happened when unloading for each specimen. So the SFRC shear wall specimens were approximately elastic at this period. When the diagonal cracks appeared on the web, the rigidity of SFRC shear wall specimens degraded slightly, the load bearing capacity grew steadily, and the residual displacement appeared gradually. Therewith, as the diagonal cracks developed larger and deeper, the reinforcements in the web yielded gradually, the pinching effect of the hysteretic curves was more obvious. Before P_m, the unloading stiffness was roughly equal to the initial loading stiffness. After P_m, the obvious degradation of stiffness and strength happened because of the crushing and spalling of concrete, and the residual displacement was more significant. The load reduced significantly as the cycle number at the same displacement level increased.

With the increasing of steel fiber volume fraction from 0% to 1.5%, the maximum load and residual deflection of SFRC shear wall specimen under each loading increment and the loading cycle number increased, which indicated the plumper hysteretic curve and better energy dissipation capacity at the same rotation level. For instance, the loading cycle number of SS-1.0-05-CF60, SS-1.0-10-CF60 and SS-1.0-15-CF60 increased by 15.38%, 30.77% and 46.15% compared with that of specimen SS-1.0-00-C60, respectively. At the same time, the larger the steel fiber volume fraction, the more slowly the hysteretic curve decreased after P_m. Moreover, the hysteretic curve of SFRC shear wall specimen decreased more rapidly after P_m with the enhancing of concrete strength, which indicated that higher concrete strength leads to worse ductility capacity. This is similar with the results in literature (Liao *et al*. 2009, Zhao *et al*. 2009).

3.3 P-Δ envelope curves

The P-Δ curve was the enveloping line of the hysteretic curve. The effect of steel fiber volume fraction on P-Δ# envelope curves is given in Fig. 9(a) according to the test results. It could be found that steel fiber volume fraction affected the P_m, corresponding peak displacement (Δ_m) and changing trend of curve. The P_m and Δ_m increased with the increase of steel fiber volume fraction. Compared with the P_m and Δ_m of specimen SS-1.0-00-C60, the P_m of SS-1.0-05-CF60, SS-1.0-10-CF60 and SS-1.0-15-CF60 increased by 4.43%, 12.71% and 18.62%, respectively; the Δ_m of SS-1.0-05-CF60, SS-1.0-10-CF60 and SS-1.0-15-CF60 increased by 19.85%, 53.44% and 67.18%, respectively. Meanwhile, the hysteretic curve decreased more slowly after P_m and was smoother with the increase of steel fiber volume fraction, indicating the load carrying capacity degradation became more slowly after P_m. It was due to the facts that higher steel fiber volume fraction could better increase the toughness of concrete and decrease its brittleness, improve the bond property between steel bar and concrete in the web, restrain the development of the diagonal cracks to a certain extent, and increase the ductility and load carrying capacities of tested specimens.

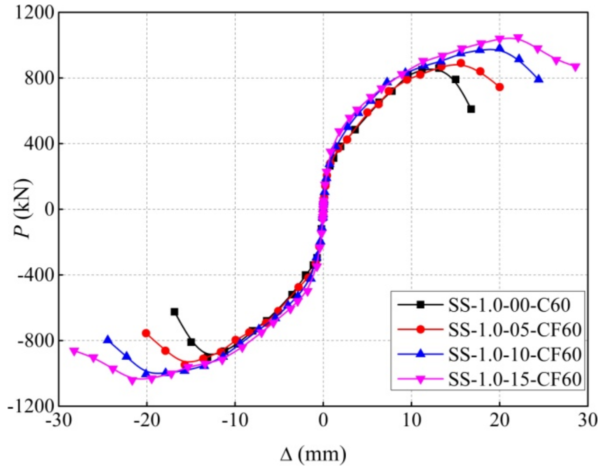

(a) Effect of steel fiber volume fraction on P-Δ envelope curves

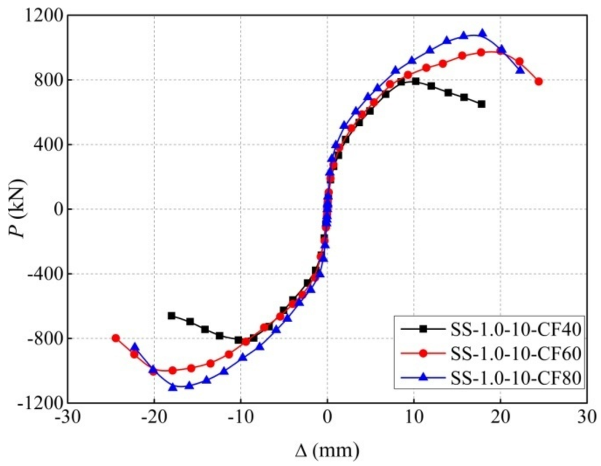

(b) Effect of concrete strength on P-Δ envelope curves

Fig. 9 Comparisons of P-Δ envelope curves

The influence of concrete strength on P-Δ#envelope curves is given in Fig. 9(b). It could be found that higher concrete strength often led to larger P_m but steeper curve after P_m. Compared with the P_m of specimen SS-1.0-10-CF40, the P_m of SS-1.0-10-CF60 and SS-1.0-10-CF80 increased by 23.97% and 36.95%, respectively; but their hysteretic curves after P_m became more and more steep. It was attributed to the fact that higher concrete strength

Table 6 Load and displacement at yield, peak and ultimate state

Specimen designation	P_y (kN)	Δ_y (mm)	P_m (kN)	Δ_m (mm)	P_u (kN)	Δ_u (mm)	μ	E_c (kN·m)
SS-1.0-00-C60	710	7.4	881	13.1	749	15.5	2.1	86.9
SS-1.0-05-CF60	748	8.3	920	15.7	782	19.4	2.3	112.9
SS-1.0-10-CF60	807	8.8	993	20.1	844	23.5	2.7	157.9
SS-1.0-15-CF60	848	9.5	1045	21.9	888	27.2	2.9	286.4
SS-1.0-10-CF40	642	5.4	801	10.3	680	16.5	3.1	82.0
SS-1.0-10-CF80	882	8.7	1097	17.9	932	21.1	2.4	162.6

would induce the larger brittleness of concrete and more obvious shear failure. Accordingly, the P_m increased, but the load carrying capacity degradation became more quickly after P_m with the enhancing of concrete strength from CF40 to CF80.

The measured loads and displacements at yield, peak and ultimate state are listed in Table 6. Due to the yield point was not obvious on P-Δ envelope curve, the yield load (P_y) and yield displacement (Δ_y) were calculated by an equal energy method (Hu *et al*. 2016), as shown in Fig. 10.

In Table 6, P_m was the mean value of positive and negative maximum loads, and Δ_m was the corresponding displacement. The P_u was 85% of P_m, and Δ_u was the corresponding lateral displacement.

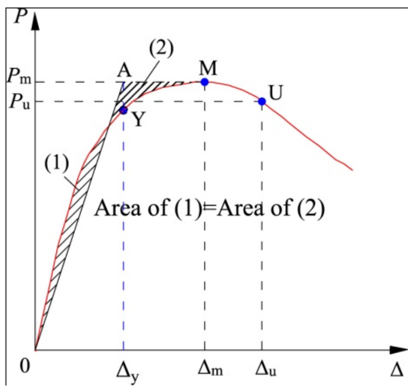

Fig. 10 Determination of the yield point

From Table 6, it could be found that, the yield, peak and ultimate loads and the corresponding lateral displacements of specimens all increased with the increasing of steel fiber volume fraction, indicating that steel fiber could improve the bearing and deformation capacities of RC shear wall specimens. For instance, compared with the P_y and Δ_y of specimen SS-1.0-00-C60, the P_y of SS-1.0-05-CF60, SS-1.0-10-CF60 and SS-1.0-15-CF60 increased by 5.35%, 13.66% and 19.44%, respectively; the Δ_y of SS-1.0-05-CF60, SS-1.0-10-CF60 and SS-1.0-15-CF60 increased by 12.16%, 18.92% and 28.38%, respectively. The yield, peak and ultimate loads of the specimens all increased with the increase of concrete strength. For instance, compared with the P_y of specimen SS-1.0-10-CF40, the P_y of SS-1.0-10-CF60 and SS-1.0-10-CF80 increased by 25.70% and 37.38%, respectively.

3.4 Ductility coefficient

The measured results of Δ_y and Δ_u for each specimen are listed in Table 6. The displacement ductility coefficient (μ) was obtained by $\mu = \Delta_u / \Delta_y$, its calculated value for each specimen is presented in Table 6.

From Table 6, it could be found that μ of all tested specimens was within the range of 2.1~3.1, which was similar with the result in literature (Liao *et al*. 2009),

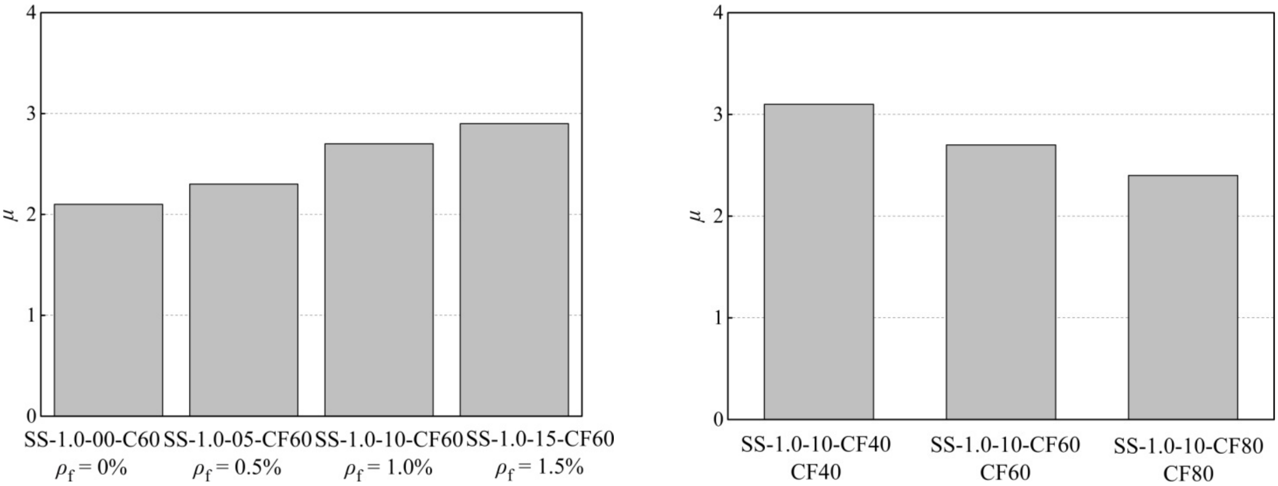

(a) Effect of steel fiber volume fraction (ρ_f) (b) Effect of concrete strength

Fig. 11 Comparisons of displacement ductility coefficient (μ)

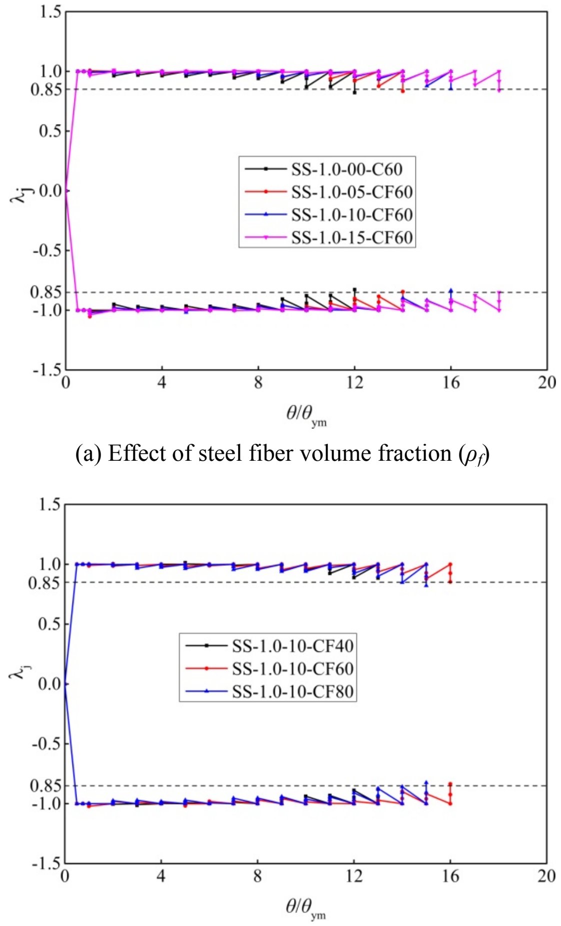

(a) Effect of steel fiber volume fraction (ρ_f)

(b) Effect of concrete strength

Fig. 12 Comparisons of strength degradation coefficient (λ_j)

indicated that SFRC shear wall with CFST columns had better ductility, and could be used as a lateral-resistance system for high-rise building.

The influences of steel fiber volume fraction and concrete strength on the μ of SFRC shear wall specimens are given in Figs. 11(a)-(b). It could be found from Fig. 1(a) that, the μ improves with the increasing of steel fiber volume fraction. Compared with the μ of specimen SS-1.0-00-C60, the μ of SS-1.0-05-CF60, SS-1.0-10-CF60 and SS-1.0-15-CF60 increased by 9.52%, 28.57% and 38.10%, respectively. From Fig. 11(b) it could be found that, the μ reduces with the enhancing of concrete strength. Compared ith the μ of specimen SS-1.0-10-CF40, the μ of SS-1.0-10-CF60 and SS-1.0-10-CF80 decreased by 12.90% and 22.58%, respectively.

3.5 Strength degradation

Because of the cumulative damage in the specimens under cyclic loading, the load-carrying capacities of the specimens decreased from one cycle to the next at the same displacement level. A strength degradation coefficient (λ_j) is used to quantify the degradation of strength, and can be defined as

$$\lambda_j = P_{i,j} / P_{1,j} \tag{2}$$

where $P_{1,j}$ and $P_{i,j}$ are the maximum load at the first cycle and the ith cycle under the jth displacement level, respectively.

The comparison of the change of the λ_j during the test of shear wall specimens with different steel fiber volume fraction or concrete strength is shown in Figs. 12(a)-(b). Table 7 shows the λ_j at typical loading stages. It could be found that the λ_j generally reduced as the lateral displacement increased, and λ_j of third cycle was smaller than that of second cycle at the same displacement level. From Fig. 12 and Table 7 it could be found that, the λ_j decreased more slowly with the increasing of steel fiber volume fraction or decrease of concrete strength.

3.6 Rigidity degradation

The lateral rigidity of SFRC shear wall specimen at each displacement level can be calculated as

Table 7 Strength degradation coefficients at different stage

Specimen designation	Loading cycle	$P_y < P < P_m$		$P_m \le P < P_u$	
		λ_j	θ/θ_{ym}	λ_j	θ/θ_{ym}
SS-1.0-00-C60	Second	0.97~0.94	8~11	0.93~0.92	11~13
	Third	0.95~0.87		0.87~0.82	
SS-1.0-05-CF60	Second	0.97~0.96	9~13	0.93~0.92	13~15
	Third	0.96~0.91		0.88~0.84	
SS-1.0-10-CF60	Second	0.99~0.96	10~15	0.94~0.92	15~17
	Third	0.97~0.91		0.90~0.84	
SS-1.0-15-CF60	Second	1.00~0.96	10~16	0.95~0.92	16~19
	Third	0.99~0.92		0.92~0.85	
SS-1.0-10-CF40	Second	0.99~0.98	7~10	0.97~0.94	10~14
	Third	0.99~0.95		0.95~0.88	
SS-1.0-10-CF80	Second	0.96~0.94	9~14	0.91~0.90	14~16
	Third	0.94~0.89		0.85~0.82	

$$K_j = \sum_{1}^{3} P_{i,j} \Big/ \sum_{1}^{3} \Delta_{i,j} \tag{3}$$

where K_j is the lateral rigidity at the jth displacement level, $P_{i,j}$ is the maximum load at the ith cycle of the jth displacement level, and $\Delta_{i,j}$ is the top displacement corresponding to $P_{i,j}$.

The relationships between the rigidity degradation and relative rotation angle (θ/θ_{ym}) for SFRC shear wall are shown in Figs. 13(a)-(b) according to the test results. From Fig. 13(a) it could be found that, as the steel fiber volume fraction increased, the initial lateral rigidity of SFRC shear wall specimens increased generally, the rigidity degradation curve became smoother, indicating that the rigidity egradation became more slowly. Compared with the initial lateral rigidity of specimen SS-1.0-00-C60, the initial lateral rigidity of SS-1.0-05-CF60, SS-1.0-10-CF60 and SS-1.0-15-CF60 increased by 2.00%, 6.31% and 10.89%, respectively. From Fig. 13(b) it could be found that, as concrete strength enhanced, the initial lateral rigidity of SFRC shear wall specimens increased generally, and the rigidity degradation showed more severe for the SFRC shear wall specimen with higher concrete strength. Compared with the initial lateral rigidity of specimen SS-1.0-10-CF40, the initial lateral rigidity of SS-1.0-10-CF60 and SS-1.0-10-CF80 increased by 18.30% and 25.88%, respectively.

3.7 Energy dissipation

The dissipated energy for SFRC shear wall specimens during each cycle can be defined as the area enclosed by the lateral load versus lateral displacement curve. The measured cumulative hysteretic dissipation energy (E_c) for all tested specimens are shown in Table 6. The change of the E_c with different steel fiber volume fraction or concrete strength is shown in Figs. 14(a)-(b).

As shown in Fig. 14(a), compared with the E_c of specimen SS-1.0-00-C60, as the steel fiber volume fraction increased, the E_c of SS-1.0-05-CF60, SS-1.0-10-CF60 and SS-1.0-15-CF60 increased by 29.92%, 81.70% and 229.57%, respectively. This was because the strengths at the same θ/θ_{ym} were relatively larger with a higher steel fiber volume fraction, thus the areas of the hysteretic loops were correspondingly larger, and higher steel fiber volume fraction also led to larger loading cycle number, resulting in the increase of E_c. In addition, the steel fibers pulled out

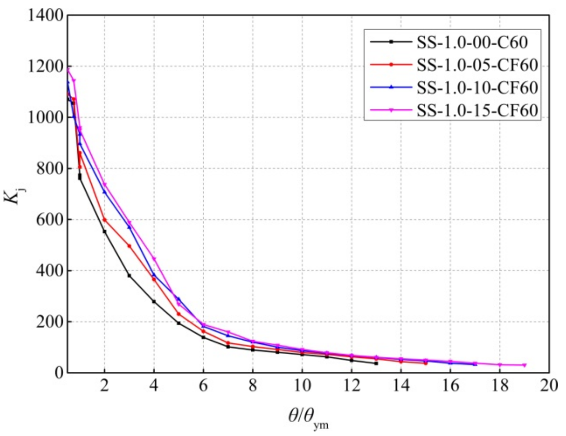

(a) Effect of steel fiber volume fraction (ρ_f) on $K_j \sim \theta/\theta_{ym}$ relations

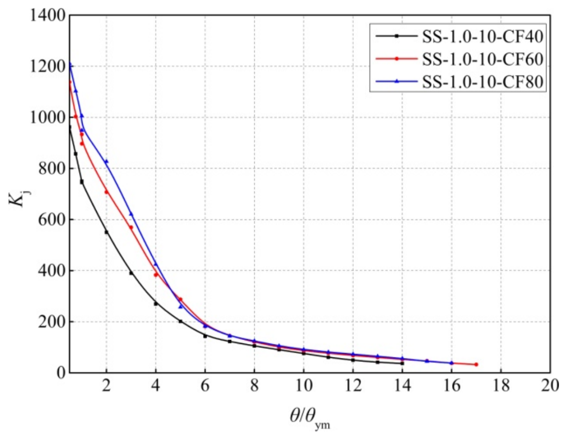

(b) Effect of concrete strength on $K_j \sim \theta/\theta_{ym}$ relations

Fig. 13 Comparisons of $K_j \sim \theta/\theta_{ym}$ relations

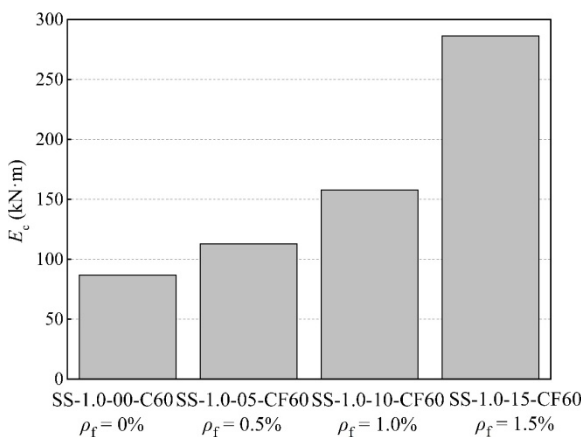

(a) Effect of steel fiber volume fraction (ρ_f)

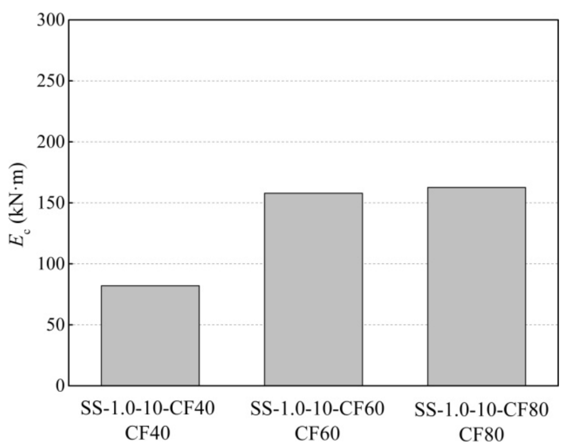

(b) Effect of concrete strength

Fig. 14 Comparisons of cumulative hysteretic dissipation energy (E_c)

constantly from concrete at the late loading stage also dissipated energy (Wille and Naaman 2012, Chen *et al.* 2015), especially after P_m, thus higher steel fiber volume fraction indicated larger E_c.

From Fig. 14(b) it could be seen that, compared with the E_c of specimen SS-1.0-10-CF40, with the enhancing of concrete strength, the E_c of SS-1.0-10-CF60 and SS-1.0-10-CF80 increased by 92.56% and 98.29%, respectively. This was due to that, the strengths at the same θ/θ_{ym} were relatively higher for specimen with a higher concrete strength, thus the areas of the hysteretic loops were correspondingly larger. However, higher concrete strength also tended to lead smaller loading cycle number as concrete strength exceeded a certain level, resulting in the light increase of the E_c, such as specimen SS-1.0-10-CF80. This is similar with the results in literature (Zhao *et al.* 2009).

4. Conclusions

This paper introduces the tests for an innovative composite shear wall named SFRC shear wall with CFST columns, and discusses the influences of experimental parameters including steel fiber volume fraction and concrete strength on the seismic performance of tested specimens. The conclusions are summarized as follows:

- The SFRC shear wall with CFST columns exhibited a distinct shear-dominant failure mode, and mainly showed a typical inclined cracking pattern during test process. Steel fibers could effectively control the crack width and improve the distribution of cracks in the web of shear wall. The cracks in the web got much thinner, more densely, more quantity and wider distribution, and the crushing and spalling of concrete also became smaller with the increasing of steel fiber volume fraction.
- The hysteretic curves of SFRC shear wall with CFST columns showed significant pinch phenomenon. The hysteretic loop became plumper and the loading cycle number became larger with the increasing of steel fiber volume fraction.
- The lateral load bearing, ductility and energy dissipation capacities increased significantly with the increasing of steel fiber volume fraction, whilst the strength and rigidity degradation became more slowly, especially after the peak load.
- The lateral load bearing and energy dissipation capacities increased obviously with the enhancing of concrete strength, whilst the influence of concrete strength on the ductility was just in reverse. In addition, the strength and rigidity degradation became more severely with the enhancing of concrete strength, particularly after the peak load.

Acknowledgments

The research described in this paper was financially supported by the National Natural Science Foundation of China (Project U1704254), and Innovative Research Team Program of Ministry of Education of China (IRT_16R67). Their financial supports are very appreciated. The authors wish to thank Mr. Ji-Yu Tang of Zhengzhou University and Mr. Hong-Bo Han of Jinan DOCER Test Machine Technology Co., Ltd for their assistance during the experiment.

References

Cai, G.C., Zhao, J., Degee, H. and Vandoren, B. (2016), “Shear capacity of steel fibre reinforced concrete coupling beams using conventional reinforcements”, *Eng. Struct.*, **128**, 428-440.

Cao, W.L., Zhang, J.W., Dong, H.Y. and Wang, M. (2011), “Research on seismic performance of shear walls with concrete filled steel tube columns and concealed steel trusses”, *Earthq. Eng. Eng. Vib.*, **10**(4), 535-546.

CECS 230:2008 (2008), Specification for design of steel-concrete mixed structure of tall buildings; Regulation of China Association for Engineering Construction Standardization, Beijing, China.

Chen, G., Hadi, M.N.S., Gao, D.Y. and Zhao, L.P. (2015), “Experimental study on the properties of corroded steel fibres”, *Constr. Build. Mater.*, **79**, 165-172.

Eltobgy, H.H. (2013), “Structural design of steel fibre reinforced concrete in-filled steel circular columns”, *Steel Compos. Struct., Int. J.*, **14**(3), 267-282.

Eom, T., Kang, S. and Kim, O. (2014), “Earthquake resistance of structural walls confined by conventional tie hoops and steel fiber reinforced concrete”, *Earthq. Struct., Int. J.*, **7**(5), 843-859.

Gao, D.Y., Zhang, L.J. and Nokken, M. (2017a), “Mechanical behavior of recycled coarse aggregate concrete reinforced with steel fibers under direct shear”, *Cement Concrete Compos.*, **79**, 1-8.

Gao, D.Y., Zhang, L.J. and Nokken, M. (2017b), “Compressive behavior of steel fiber reinforced recycled coarse aggregate concrete designed with equivalent cubic compressive strength”, *Constr. Build. Mater.*, **141**, 235-244.

GB/T 228.1-2010 (2010), Metallic materials-Tensile testing-Part 1: Method of test at room temperature, Sandardization Administration of China; Beijing, China.

Hu, H.S., Nie, J.G., Fan, J.S., Tao, M.X., Wang, Y.H. and Li, S.Y. (2016), “Seismic behavior of CFST-enhanced steel plate-reinforced concrete shear walls”, *J. Constr. Steel Res.*, **119**, 176-189.

Huang, F.Y., Yu, X.M. and Chen, B.C. (2012), “The structural performance of axially loaded CFST columns under various loading conditions”, *Steel Compos. Struct., Int. J.*, **13**(5), 451-471.

Kang, T.H.K., Kim, W., Massone, L.M. and Galleguillos, T.A. (2012), “Shear-Flexure Coupling Behavior of Steel Fiber-Reinforced Concrete Beams”, *ACI Struct. J.*, **109**(4), 435-444.

Li, N., Lu, Y.Y., Li, S. and Liang, H.J. (2015), “Statistical-based evaluation of design codes for circular concrete-filled steel tube columns”, *Steel Compos. Struct., Int. J.*, **18**(2), 519-546.

Liao, F.Y., Han, L.H. and Tao, Z. (2009), “Seismic behaviour of circular CFST columns and RC shear wall mixed structures: Experiments”, *J. Constr. Steel Res.*, **65**(8-9), 1582-1596.

Mirsayah, A.A. and Banthia, N. (2002), “Shear strength of steel fiber-reinforced concrete”, *ACI Mater. J.*, **99**(5), 473-479.

Qiao, Q.Y., Zhang, W.W., Qian, Z.W., Cao, W.L. and Liu, W.C. (2017), “Experimental study on mechanical behavior of shear connectors of square concrete filled steel tube”, *Appl. SCI-Basel*, **7**(8), 818.

Qu, X.S., Chen, Z.H. and Sun, G.J. (2015), “Axial behaviour of rectangular concrete-filled cold-formed steel tubular columns with different loading methods", *Steel Compos*. *Struct*., *Int*. *J*., **18**(1), 71-90.

Saridemir, M., Severcan, M.H. and Celikten, S. (2017), "Mechanical properties of SFRHSC with metakaolin and ground pumice: Experimental and predictive study", *Steel Compos*. *Struct*., *Int*. *J*., **23**(5), 543-555.

Shirali, N.M. (2002), "Seismic resistance of hybrid shear wall system", Ph.D. Dissertation; Darmstadt University of Technology, Germany.

Singh, S.P. and Kaushik, S.K. (2001), "Flexural fatigue analysis of steel fiber-reinforced concrete", *ACI Mater*. *J*., **98**(4), 306-312.

Tang, C.W. (2017), "Fire resistance of high strength fiber reinforced concrete filled box columns", *Steel Compos*. *Struct*., *Int*. *J*., **23**(5), 611-621.

Tang, X.R., Jiang, Y.S. and Ding, D.J. (1993), "Application of the theory of softened truss to low-rise steel fiber high strength concrete shear walls", *J. Build*. *Struct*., **14**(2), 2-11. [In Chinese]

Vetr, M.G., Shirali, N.M. and Ghamari, A. (2016), "Seismic resistance of hybrid shear wall (HSW) systems", *J. Constr*. *Steel Res*., **116**, 247-270.

Wille, K. and Naaman, A.E. (2012), "Pullout Behavior of High-Strength Steel Fibers Embedded in Ultra-High-Performance Concrete", *ACI Mater*. *J*., **109**(4), 479-487.

Xia, Z.M. and Naaman, A.E. (2002), "Behavior and modeling of infill fiber-reinforced concrete damper element for steel-concrete shear wall", *ACI Struct*. *J*., **99**(6), 727-739.

Xiao, C.Z., Cai, S.H., Chen, T. and Xu, C.L. (2012), "Experimental study on shear capacity of circular concrete filled steel tubes", *Steel Compos*. *Struct*., *Int*. *J*., **13**(5), 437-449.

Xu, C., Su, Q.T. and Masuya, H. (2017), "Static and fatigue performance of stud shear connector in steel fiber reinforced concrete", *Steel Compos*. *Struct*., *Int*. *J*., **24**(4), 467-479.

Zerbino, R.L. and Barragan, B.E. (2012), "Long-Term Behavior of Cracked Steel Fiber-Reinforced Concrete Beams under Sustained Loading", *ACI Mater*. *J*., **109**(2), 215-224.

Zhao, J. and Dun, H.H. (2014), "A restoring force model for steel fiber reinforced concrete shear walls", *Eng*. *Struct*., **75**, 469-476.

Zhao, J., Gao, D.Y. and Du, X.L. (2009), "Seismic behavior of steel fiber reinforced concrete low-rise shear wall", *Earthq*. *Eng*. *Eng*. *Vib*., **29**(4), 103-108.

CC